NANO LETTERS

pubs.acs.org/NanoLett

Letter

Achieving Boosted Thermoelectric Power Factor of MoS_2 through Selective Charged-Impurity-Free Doping

Sooyeon Moon, Jiwoo Yang, Deok Hwang Kwon, Daeheum Cho, Jae-Keun Kim, Jae Won Shim, Heesuk Kim, Takhee Lee, Hyejin Jang,* Kyungjune Cho,* and Seungjun Chung*

Cite This: *Nano Lett.* 2025, 25, 9994−10002

Read Online

ACCESS | Metrics & More | Article Recommendations | Supporting Information

ABSTRACT: Ultrathin two-dimensional (2D) transition metal dichalcogenides (TMDs) exhibit unique band structures, allowing promising thermoelectric properties. Achieving a high power factor (*PF*) for thermoelectric generators (TEGs) requires optimizing both the Seebeck coefficient (*S*) and electrical conductivity (σ). Conventional surface charge-transfer doping can be a solution to enhance σ by introducing additional electrons. However, residual organic dopants act as charged impurities, degrading charge transport and lowering *PF* due to the intensified trade-off between carrier concentration and *S*. We propose a charged-impurity-free diffusion doping method for CVD-grown molybdenum disulfide (MoS_2) to enhance *PF*. By depositing organic dopants on the contact region and enabling electron diffusion into the channel via carrier concentration gradients, σ is improved while maintaining high *S*. This approach achieves a record-high *PF* of 1698 $\mu W/mK^2$ for CVD-grown TMDs. Our strategy offers a promising pathway to enhance thermoelectric performance, not limited by the exacerbated trade-off relationship observed in conventional doping methods.

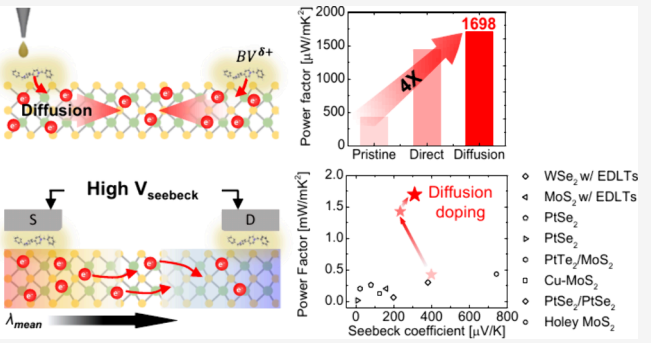

KEYWORDS: *thermoelectric, 2D transition metal dichalcogenides, diffusion, charged-impurity-free doping, Seebeck coefficient*

Atomically thin two-dimensional (2D) transition metal dichalcogenides (TMDs) have attracted significant attention for their promising electrical properties.[1−7] Recently, their unique quantum confinement effects, which result in a sharp density of states, large effective mass, and high valley degeneracy, have extended their potential to thermoelectric generators (TEGs).[8−10] TEG is one of the most promising energy harvesters that convert waste heat into electricity when there is a temperature difference across the thermoelectric (TE) legs.[11−17] To achieve high TE efficiency, it is crucial to maximize both the Seebeck coefficient (*S*) and electrical conductivity (σ), as the TE power factor (*PF*) is defined by the relationship $PF = S^2\sigma$, following the Mott formula.[18,19] Because these parameters are closely correlated, efforts have been dedicated to optimizing both *S* and σ to enhance the *PF* by carefully controlling charge transport properties, such as charge carrier mobility (μ) and concentration (*n*).

Owing to the wide tunability of charge transport properties associated with an inherently high *S* of up to 30 mV/K, molybdenum disulfide (MoS_2) has been intensively studied as a TE leg for realizing high-performance TEGs.[20−24] However, their relatively poor σ attributed to grain boundaries and their environmental instability are bottlenecks in the realization of high-performance TEGs with lower *PF* values.[25,26] To address this, many doping strategies that introduce additional charge carriers into the TE legs have been explored as effective solutions.[27−29] Among them, nondestructive surface charge-transfer doping (SCTD) has emerged as a promising candidate for enhancing the σ of 2D TMDs. This approach leverages the ultrathin nature of MoS_2, where charge carrier transfer from organic dopants can modulate its electrical properties effectively.[30−32] However, SCTD has a critical limitation in TE applications: in addition to the inevitable *n*-*S* trade-off, remaining charged impurities on the atomically thin channels impede charge transport, further intensifying the trade-off and sharply lowering *S*. When an organic dopant donates electrons to MoS_2, it becomes positively charged and acts as a Coulomb scattering center, leading to μ degradation. Because of the high surface sensitivity of 2D materials, charged impurity scattering can severely impact on charge carrier transport, ultimately reducing both σ and *S*.[33,34] To overcome these drawbacks, various strategies have been proposed to minimize the

Received: March 13, 2025
Revised: June 4, 2025
Accepted: June 6, 2025
Published: June 12, 2025

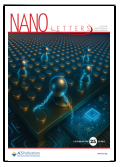

https://doi.org/10.1021/acs.nanolett.5c01649
Nano Lett. 2025, 25, 9994−10002

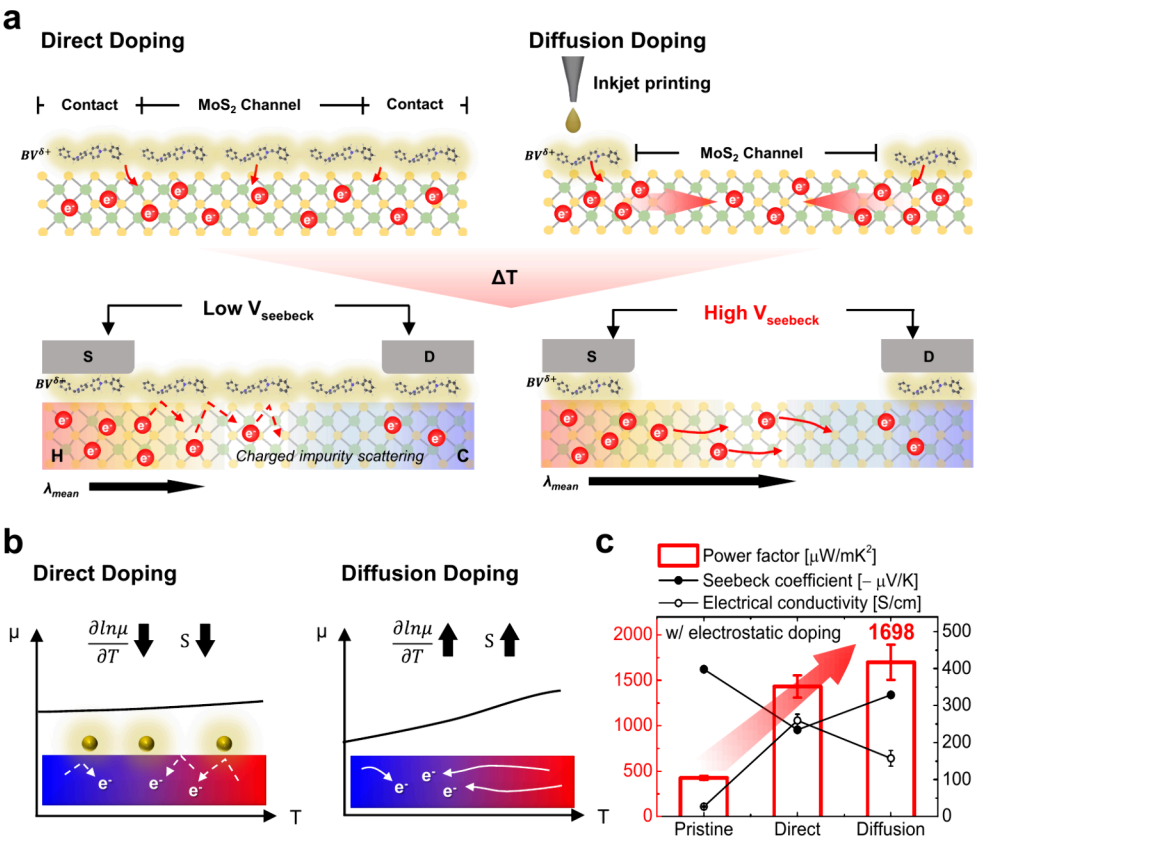

Figure 1. Enhanced TE properties of diffusion-doped MoS_2 TEGs. (a) Doping mechanisms of the direct- and diffusion-doped MoS_2 TEGs. (b) Illustration of temperature-dependent mobility and Seebeck coefficient derived using different doping methods. (c) Improved power factor of diffusion-doped MoS_2 TEGs with optimized electrical conductivity and Seebeck coefficient.

detrimental effects of charged impurities and maintain efficient charge transport.[35−37]

In this regard, we propose a diffusion-mediated modulation doping approach (hereafter referred to as diffusion doping) to significantly enhance the TE *PF* of large-area 2D MoS_2. Modulation doping spatially separates free carriers from their parent dopant species, effectively mitigating impurity-induced scattering and enabling high carrier mobility. Moreover, the diffusion doping method could be achieved by selectively depositing dopants onto the contact regions of large-area 2D MoS_2 films using inkjet printing, which allows high reproducibility and significant potential as a scalable fabrication process. It significantly improves σ while avoiding charged impurity scattering in the TE legs. We characterized the temperature-dependent electrical properties of the doped films, demonstrating that this approach mitigates the undesirable reduction in *S* after SCTD. By optimizing the doping conditions and device architecture, we achieved the highest reported *PF* of 1698 $\mu W/mK^2$ for CVD-grown MoS_2. This strategy provides a scalable and effective pathway for realizing high-performance thermoelectric devices based on 2D TMDs.

Figure 1a shows a schematic of the direct SCTD and diffusion SCTD methods for large-area MoS_2. Compared to the conventional direct doping method, where organic molecules are directly deposited onto the whole area of MoS_2 TE leg, the proposed diffusion doping method was conducted through the selective deposition of highly concentrated benzene viologen (BV) dopant only on the contact region of MoS_2 via inkjet printing (Figures S1 and S2). Notably, we observed no significant impact of the surface roughness of the inkjet-printed BV layers on the effectiveness of diffusion doping in the underlying MoS_2 film.[38−40] This doping reliability under surface roughness is attributed to the local carrier redistribution within the BV-deposited contact region of MoS_2. BV is a well-known dopant for chemical doping in TMDs, acting as an electron donor due to the energy level difference between its reduction potential and the conduction band edge of TMDs.[41−44] Excessive electrons in the contact region transferred from the selectively deposited BV molecular dopants promote diffusion into the channel region, increasing the electron concentration in the TE legs gradually. In contrast, for direct SCTD, electrons are transferred from the BV dopants into the TE leg, after which the remaining dopants act as charged impurities, serving as centers of Coulomb scattering once they have donated electrons. This long-range scattering significantly limits carrier transport in atomically thin 2D TMDs, where surface interfacial properties play a crucial role. Consequently, most experimentally reported mobilities are substantially lower than the theoretically predicted values.[45,46]

As aforementioned, maximizing the power factor ($PF = S^2\sigma$) with optimized *S* and σ is essential for high-performance TEGs. In the Mott relationship, *S* is expressed as follows:

$$S = \frac{\pi^2}{3}\frac{k_B^2 T}{e}\left[\frac{\partial \ln\sigma(\varepsilon)}{\partial \varepsilon}\right]_{\varepsilon=\varepsilon_F} = \frac{\pi^2}{3}\frac{k_B^2 T}{e}\left[\frac{1}{n}\frac{\partial n(\varepsilon)}{\partial \varepsilon} + \frac{1}{\mu}\frac{\partial \mu(\varepsilon)}{\partial \varepsilon}\right]_{\varepsilon=\varepsilon_F} \quad (1)$$

where μ is the carrier mobility, *e* is the carrier charge, *T* is the absolute temperature, k_B is the Boltzmann constant, and ε_F is the Fermi energy.[47] The σ can be defined as follows:

https://doi.org/10.1021/acs.nanolett.5c01649
Nano Lett. 2025, 25, 9994−10002

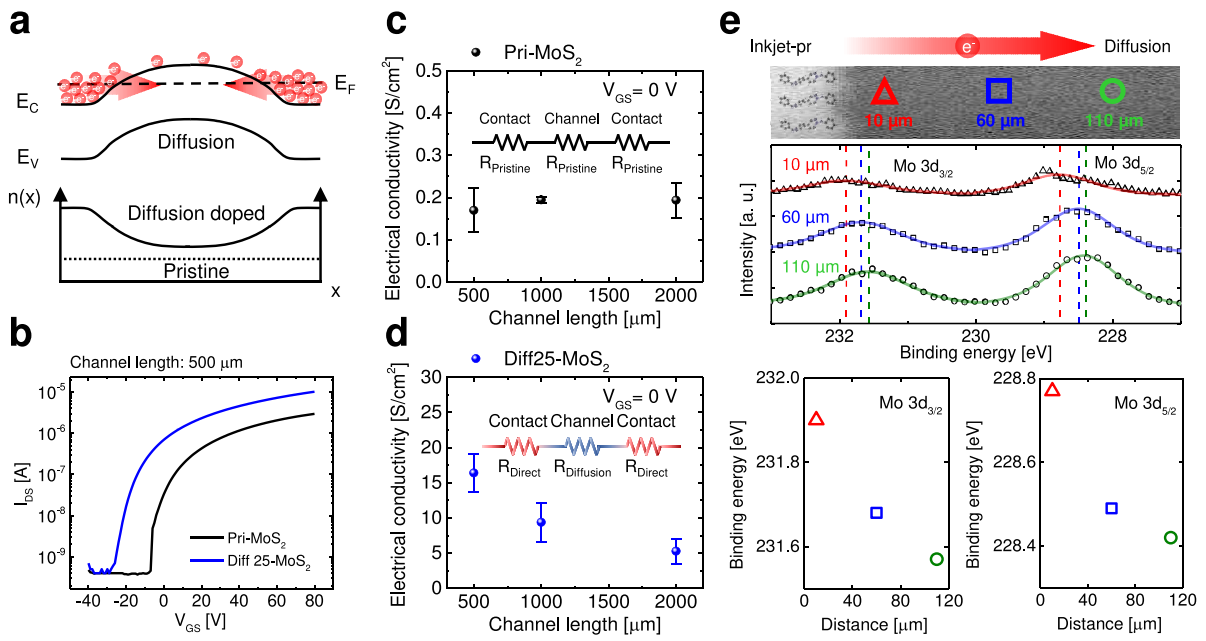

Figure 2. Electrical properties of pristine and diffusion-doped MoS_2 FETs. a) Illustration of band structure and carrier concentration for diffusion doping. (b) $I_{DS}-V_{GS}$ curves of Pri-MoS_2 and Diff 25-MoS_2 FETs as a function of back-gate voltage. (c, d) Electrical conductivities of (top) Pri-MoS_2 and (bottom) Diff 25-MoS_2 FETs as a function of channel length. (e) XPS spectra of the Diff-MoS_2 FET as a function of distance from the BV inkjet-printed contact region.

$$\sigma = ne\mu\left(\mu = \frac{e\tau}{m^*}\right) \tag{2}$$

where n, τ, and, m^* represent the carrier concentration, relaxation time and effective mass, respectively. Given the equations, we can assume that not only controlling the n but also modulating μ is highly critical for enhancing the both S and σ. By replacing $1/\partial\varepsilon$ with $1/k_B\partial T$ in eq 1, it is noteworthy that securing the gradient of μ with respect to T can lead to an increase in the S value. In this regard, the additional charged impurities from direct doping can enhance scattering, leading to a suppressed gradient of μ as a function of T and deteriorating S, as shown in Figure 1b. Therefore, reducing the scattering of charged impurities is crucial for achieving high TE performance. In this regard, the diffusion doping method is advantageous for achieving high S values by controlling the n and μ of large-area MoS_2 TEGs, which leads to an approximately 18.7% enhancement in PF compared to TEGs employing conventional direct SCTD under equivalent dopant conditions (Figure 1c).

Diffusion doping is accomplished by establishing a carrier concentration gradient between the contact and channel regions. By selectively depositing a high concentration of BV molecules onto the contact regions of a large-area MoS_2 film, a 3D (BV molecules)−2D (MoS_2) multidimensional heterostructure is formed, creating a strong electron concentration gradient that facilitates the diffusion of excess electrons into the channel region. This mechanism is further supported by previous research by Ferney A. Chaves et al., which demonstrated the diffusion of charge carriers in 2D materials across heterostructures.[48] In addition, carrier diffusion into the MoS_2 channel could be significantly enhanced under an applied V_{DS}, as the built-in potential barriers - both between BV molecules and MoS_2 contact region, and between the contact and channel - could be also reduced. Based on this, as illustrated in Figure 2a, we assumed excess electrons could travel relatively long distances without introducing charged impurities on the MoS_2 surface, as evidenced by the electrical characteristics of diffusion-doped MoS_2.

To evaluate the diffusion doping effects, we measured the electrical characteristics of large-area MoS_2 FETs with various doping conditions and different channel lengths. Comprehensive imaging analyses using SEM and OM were conducted to confirm the absence of BV molecules on the channel area, as shown in Figures S3 and S4. During this experiment, a minimal gate leakage current in the range of several tens of picoamperes was observed (Figure S5), and tens of MoS_2 FETs with different channel lengths were measured to ensure the accuracy of the electrical characterization. While BV is deposited only at the contact regions, with no dopants on the channel surface, doping effect is observed, resulting in higher field-effect mobility (μ_{FET}), on-state current (I_{ON}), and n, as shown in Figure 2b, which is consistent with previous results.[49] In particular, effective doping concentration (Δn_{dop}) of diffusion-doped MoS_2 with BV concentration of 25 mg/mL (Diff 25-MoS_2) is similar to that of direct-doped MoS_2 FETs with BV concentration of 5 mg/mL (Direct 5-MoS_2) (Figure S6). The total resistance of diffusion-doped MoS_2 (Diff-MoS_2) FETs is low and increases exponentially with channel length, compared to pristine MoS_2 (Pri-MoS_2) FETs, which exhibit high total resistance that increases linearly with channel length (Figure S7). This result is attributed to the exponentially decreasing n across the channel length of the diffusion-doped FETs as the distance from the direct-doped contact region increases, whereas the n remains constant in Pri-MoS_2 FETs. Notably, this carrier density gradient becomes negligible with increasing levels of electrostatic doping (Figure S8). In this regard, the Diff-MoS_2 FETs show an exponential decrease in σ with increasing channel length, whereas Pri-MoS_2 maintains consistent regardless of channel length, confirming the quality and uniformity of the MoS_2 film (Figure 2c, d).

https://doi.org/10.1021/acs.nanolett.5c01649
Nano Lett. 2025, 25, 9994−10002

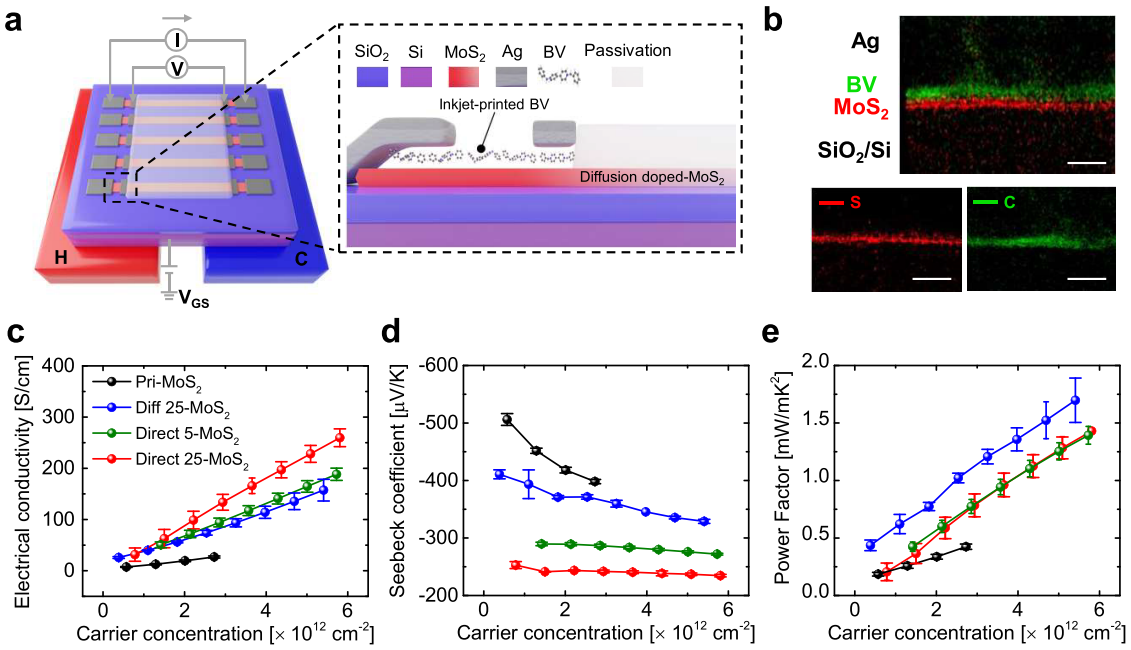

Figure 3. TE properties of large-area MoS_2 TEGs. (a) Schematic of the diffusion-doped MoS_2 TEG structure. (b) Cross-sectional EFTEM images (scale bar: 50 nm). (c–e) Electrical conductivity, Seebeck coefficient, and power factor as functions of carrier concentration under different doping conditions. Diffusion doping achieves a power factor of approximately 1698 $\mu W/mK^2$, with a suppressed Seebeck coefficient reduction from about −250 to −350 $\mu V/K$.

To accurately compare the contact resistance (R_C) between Pri-MoS_2 and Diff-MoS_2 devices, we modified the conventional transmission line method (TLM) approach, referred to here as the "modified TLM." Under this model, the total resistance is given by

$$R_{total} = 2R_c + R_{Direct}L_{ch} + (R_{pristine} - R_{Direct})L_N(1 - e^{-L_{ch}/L_N})$$

Here, R_C is the contact resistance, while $R_{Pristine}$ and R_{Direct} denote the resistance per unit length of the pristine and direct-doped channel regions, respectively. L_{Ch} is the total channel length, and L_N is the characteristic diffusion length (refer to Supporting Information for details). As shown in Figure S9, diffusion doping significantly lowers R_C compared to the Pri-MoS_2, confirming a substantial reduction in R_C.

When BV molecules donate additional electrons to MoS_2, the characteristic X-ray photoelectron spectroscopy (XPS) peaks of MoS_2 shift toward higher binding energies, indicating that the Fermi level moves closer to the conduction band edge.[50] As the distance from the contact region increases, the Mo $3d_{3/2}$ and Mo $3d_{5/2}$ peaks of the Diff-MoS_2 FETs shift toward lower binding energies, with a corresponding decrease in n (Figure 2e). Additionally, the absence of N-peaks in the diffusion-doped channel (Figure S10) confirms no BV molecules on the MoS_2 surface. Despite this, a strong doping effect is observed, leading to enhanced μ and n in Diff-MoS_2 FETs.

Figure 3a shows a schematic of the diffusion-doped TEGs fabricated by selective inkjet printing. Energy-filtered transmission electron microscopy (EFTEM) images (Figure 3b) confirm the absence of significant damage to the BV layers during the Ag ink printing for the contact deposition. The MoS_2 TEGs have four contacts for gated four-point probe measurements, ensuring reliable TE and electrical characterization while minimizing contact resistance in 2D devices (Figures S11 and S12).[51] The σ of both direct-doped and diffusion-doped TEGs increased dramatically compared to that of pristine TEGs, as displayed in Figure 3c. Pri-MoS_2 TEGs exhibited the S values from −500 to −400 $\mu V/K$, similar to CVD-grown MoS_2 films reported in previous works.[52,53] As n increased following electrostatic doping or a higher dopant concentration, the S value of doped MoS_2 TEGs decreased due to the conventional trade-off relationship between n and S.[54,55] For the Direct-MoS_2, S is further suppressed up to approximately −250 $\mu V/K$ (Figure 3d). Notably, the Diff-MoS_2 TEGs exhibit a considerably lower S reduction (−350 $\mu V/K$) than that of the Direct-MoS_2, despite a similar range of n. These results strongly suggest that S is not solely determined by the n of 2D TE materials. Instead, charge-carrier transport properties should also be carefully considered to achieve high S values.

As depicted in Figure 3e, PF, attributed to the squared influence of the S, is higher for doped MoS_2 TEGs than that of Pri-MoS_2 TEGs due to the enhanced σ. Specifically, Diff 25-MoS_2 achieve an average PF of 1698 $\mu W/mK^2$, an 18.7 % improvement over direct-doped TEGs, achieving the highest reported value. Although direct-doped MoS_2 with the BV concentration of 25 mg/mL (Direct 25-MoS_2) TEGs demonstrate the highest σ and Δn_{dop}, their PF is lower than that of diffusion-doped ones due to their significantly reduced S, as further supported by the DFT analysis in Figures S13–S15. Moreover, while σ value of Direct 25-MoS_2 surpasses those of direct-doped TEGs with lower dopant concentrations, their PF values are similar. This suggests that the conventional direct SCTD strategy with increased n faces intensified trade-off between enhanced σ and reduced S, limiting PF values. Consequently, maximizing TE efficiency requires optimizing S, as well as maximizing σ, by systematically considering charge carrier transport properties affected by unwanted charged impurities.

https://doi.org/10.1021/acs.nanolett.5c01649
Nano Lett. 2025, 25, 9994−10002

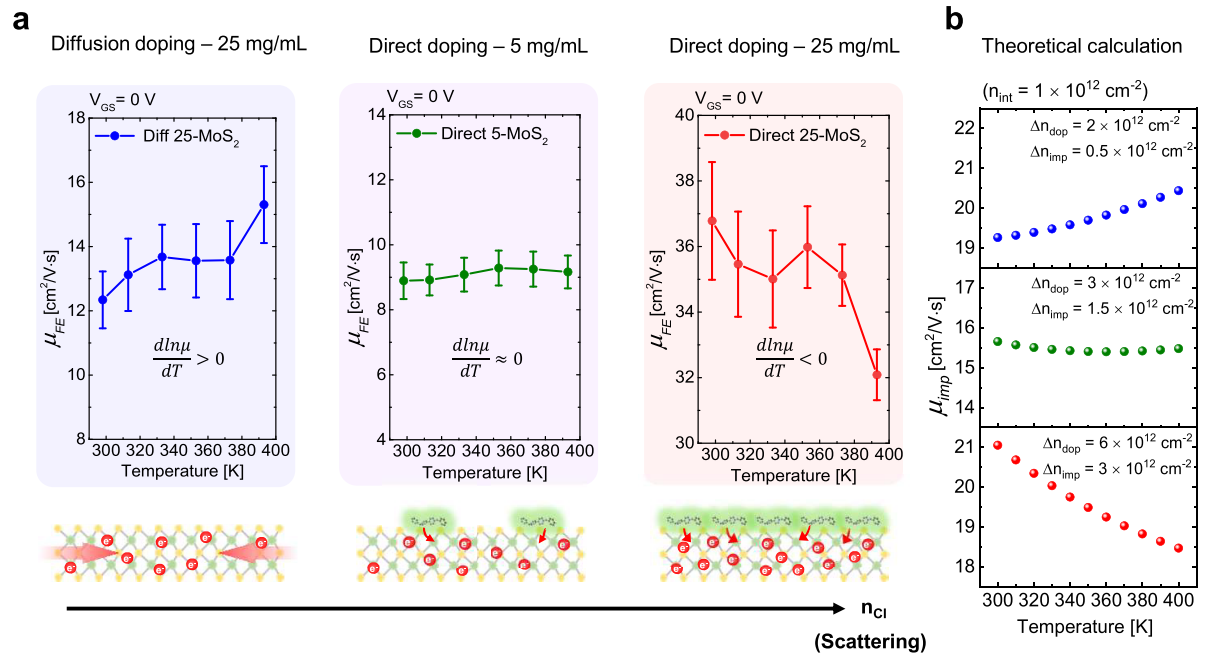

Figure 4. Characterization of temperature-dependent mobility and theoretical calculations. (a) Temperature-dependent mobility of (left) Diff 25-MoS_2, (middle) Direct 5-MoS_2, and (right) Direct 25-MoS_2 TEGs with schematic images of MoS_2 channel. (b) Theoretical calculations of charged impurity limited mobility as a function of temperature.

Based on Mott's equation, not only the value of μ itself but also distinctly different mobilities at the TE leg ends under a temperature gradient, a large positive value of temperature-dependent mobility ($d\mu/dT$), can result in high S.[56] Since charged impurity is one of the most predominant factor determining the μ of 2D materials, we examined its impact on $d\mu/dT$, focusing on the charged impurity scattering-limited mobility (μ_{imp}) using the screened charged impurity scattering model. According to Hwang et al., this model has been studied both theoretically and experimentally to understand the competition between charge-carrier screening and charged-impurity scattering in 2D materials.[57] The screening effect enhances μ by reducing the Coulomb potential of charged impurities through charge carriers, while impurity scattering lowers μ due to the pronounced influence of charged impurities on the channel surface.[58,59] Moreover, there is a critical temperature dependence of S beyond the Mott formula, arising from temperature-dependent screening and scattering effects. As the temperature increases, screening strengthens due to thermally excited carriers, while scattering intensifies with additional kinetic energy from the thermal energy. The dominant contribution in this competition governs μ changes with temperature and depends on the charged impurity concentration. From this observation, we can assume that a high charged impurity concentration enhances scattering, reducing $d\mu/dT$, whereas minimizing impurities allows screening to dominate, increasing $d\mu/dT$. Therefore, we explored temperature-dependent field-effect mobility ($d\mu_{FE}/dT$) in MoS_2 TEGs under three conditions—Diff 25-MoS_2, Direct 5-MoS_2, and Direct 25-MoS_2 by varying effective doping concentration (Δn_{dop}) and charged impurity concentration (Δn_{imp}).

As described in the left panel in Figure 4a, field-effect mobility (μ_{FE}) of the Diff 25-MoS_2 TEGs increases with temperature, indicating a positive $d\mu_{FE}/dT$. This trend is expected due to a dominant screening effect resulting from thermally generated charge carriers with no additional charged impurities introduced during doping. For direct doping, the rate of increase in μ *versus* temperature is suppressed. As discussed, despite similar doping effects at 300 K of Direct 5-MoS_2 and Diff 25-MoS_2, Direct 5-MoS_2 shows smaller $d\mu_{FE}/dT$, likely due to stronger scattering from charged impurities on the channel. In the case of Direct 25-MoS_2 TEGs, the highest μ_{FE}, indicative of strong screening effect from high Δn_{dop}, decreases with temperature, (right panel of Figure 4a), suggesting extremely high Δn_{imp} can induce strong charged impurity scattering and negative $d\mu_{FE}/dT$. Furthermore, due to the strong screening effect from the high Δn_{dop} region, the increase in μ caused by the screening effect from thermally excited charge carriers appears relatively less effective. From these observations, we can infer that S reduction strongly depends on doping methods (Figure 3), which can be attributed to the values of $d\mu/dT$ with the different Δn_{imp}. Diff-MoS_2 TEGs, with positive $d\mu/dT$, exhibit the highest S, whereas Direct 25-MoS_2 TEGs, with negative $d\mu/dT$, lead to the lowest S. Despite similar screening efficiency by Δn_{dop}, Direct 5-MoS_2 TEGs exhibit lower S than Diff 25-MoS_2 TEGs due to increased charged impurity scattering reducing $d\mu/dT$. This is further supported by the theoretical calculations in Figure 4b. In this theoretical model, the temperature-dependence of charged impurity scattering-limited mobility ($d\mu_{imp}/dT$) is calculated by controlling Δn_{imp} and Δn_{dop}, based on screened charge impurity scattering model. For a fair comparison, all cases use the same pristine carrier density (n_{int}), representing the n of MoS_2 before doping. Additional details on the theoretical model are provided in Section 6 of Supporting Information.

As expected from the experimental data, for similar Δn_{dop}, a lower Δn_{imp} leads to a higher $d\mu_{imp}/dT$. Conversely, extremely high Δn_{dop} and Δn_{imp} reduce $d\mu_{imp}/dT$ to a negative value, aligning with our experimental results. Consequently, it implies that the optimization of $d\mu/dT$ through minimizing Δn_{imp}

https://doi.org/10.1021/acs.nanolett.5c01649
Nano Lett. 2025, 25, 9994−10002

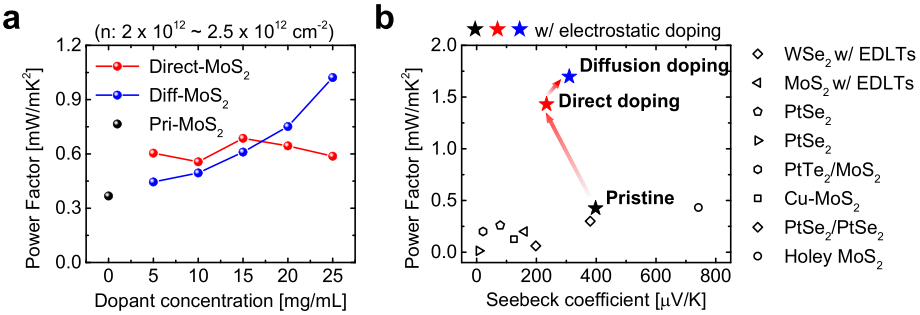

Figure 5. TE power factor of large-area MoS_2 TEGs. (a) Power factor as a function of dopant concentration of Pri-MoS_2, Direct-MoS_2, and Diff-MoS_2 TEGs. (b) Improved TE power factor compared with previous results for large-area CVD-grown 2D TEGs.

through diffusion doping can be a key pathway for enhancing TE performance. These findings indicate that conventional direct doping, while effective in improving σ of large-area 2D TMDs, has a critical limitation in enhancing the TE performance owing to the significant reduction in S.

We analyzed PF as a function of dopant concentration for the direct and diffusion doping methods (Figure 5a). To investigate the effects of charged impurities on PF, the evaluation must be conducted under similar screening condition. As shown, both methods enhance σ through charge-carrier injection from the deposited BV dopants, exhibiting an increase in PF compared with the Pri-MoS_2 TEGs. However, in Direct-MoS_2 TEGs, the PF remains nearly constant with increasing dopant concentration due to a significant reduction in S caused by increase in Δn_{imp} and the resulting gradual decline in $d\mu/dT$ caused. In contrast, diffusion doping improves PF with dopant concentration increasing σ without further degrading S due to positive $d\mu/dT$. This trend is consistent even under lower n range and various gating voltages (Figure S16−17). Consequently, we achieve a PF of approximately 1698 $\mu W/mK^2$ for large-area 2D MoS_2 TEGs after diffusion doping. This is the highest value recorded for large-area 2D TEGs compared to previous studies,[60−66] as shown in Figure 5b and Table S1, which explored various doping techniques and device structures to enhance the TE performance of CVD-grown 2D TMDs. To further evaluate the environmental stability of MoS_2 TEGs with diffusion doping, we examined their long-term operational reliability. Under prolonged operation over 5 days, we could not observe significant degradation of thermoelectric performance, maintaining the Seebeck coefficient. (Figure S18).

In this study, we achieved a high PF in large-area MoS_2 TEGs via diffusion doping. Using selective inkjet printing, the BV dopants were deposited only on the contact regions, and the donated electrons could then diffuse from the contact regions into the TE legs. The proposed diffusion doping significantly improved σ of the MoS_2 TE legs without resultant charged impurities onto the channel. Since S in 2D TMDs was highly influenced by $d\mu/dT$ as well as change in n, diffusion doping preserved high S by maximizing positive $d\mu/dT$, which is associated with minimizing charged impurity scattering. This observation was demonstrated by temperature-dependent electrical characterization, which showed that diffusion doping can eliminate the contribution of charge−impurity scattering, thereby mitigating the reduction of the S, as supported by theoretical calculations of doped MoS_2 TEGs. Consequently, the Diff-MoS_2 TEGs exhibited an optimized PF by enhancing the σ while maintaining high S. This strategy addressed the limitations of conventional direct doping, achieving the highest PF with an average value of 1698 $\mu W/mK^2$ for large-area 2D MoS_2. Our study provides insights into the effects of charge transport on the TE performance of 2D TMDs, emphasizing the significant impact of charged impurities in large-area 2D TMDs for TE applications.

■ ASSOCIATED CONTENT

Supporting Information

The Supporting Information is available free of charge at https://pubs.acs.org/doi/10.1021/acs.nanolett.5c01649.

Device fabrication, electrical and thermoelectric characterizations, XPS and DFT analyses, theoretical calculations, and experimental details (PDF)

■ AUTHOR INFORMATION

Corresponding Authors

Hyejin Jang − *Department of Material Science and Engineering and Research Institute of Advanced Materials, Seoul National University, Seoul 08826, Republic of Korea;* orcid.org/0000-0002-5896-684X; Email: hjang@snu.ac.kr

Kyungjune Cho − *Electronic and Hybrid Materials Research Center and Convergence Research Center for Solutions to Electromagnetic Interference in Future-mobility, Korea Institute of Science and Technology, Seoul 02792, Republic of Korea;* orcid.org/0000-0002-1382-2877; Email: kcho@kist.re.kr

Seungjun Chung − *School of Electrical and Engineering, Korea University, Seoul 02841, Republic of Korea;* orcid.org/0000-0002-4867-4149; Email: seungjun@korea.ac.kr

Authors

Sooyeon Moon − *Department of Material Science and Engineering, Seoul National University, Seoul 08826, Republic of Korea; School of Electrical and Engineering, Korea University, Seoul 02841, Republic of Korea*

Jiwoo Yang − *School of Electrical and Engineering, Korea University, Seoul 02841, Republic of Korea; Department of Electrical and Computer Engineering, Seoul National University, Seoul 08826, Republic of Korea;* orcid.org/0009-0005-6825-2452

Deok Hwang Kwon − *Center for Energy Materials Research, Korea Institute of Science and Technology, Seoul 02792, Republic of Korea*

Daeheum Cho − *Department of Chemistry, Kyungpook National University, Daegu 41566, Republic of Korea;* orcid.org/0000-0002-0322-4291

https://doi.org/10.1021/acs.nanolett.5c01649
Nano Lett. 2025, 25, 9994−10002

Jae-Keun Kim − *Max Planck Institute of Microstructure Physics, 06120 Halle, Saale, Germany*
Jae Won Shim − *School of Electrical and Engineering, Korea University, Seoul 02841, Republic of Korea;* orcid.org/0000-0001-8387-160X
Heesuk Kim − *Electronic and Hybrid Materials Research Center, Korea Institute of Science and Technology, Seoul 02792, Republic of Korea;* orcid.org/0000-0002-0898-7781
Takhee Lee − *Department of Physics and Astronomy and Institute of Applied Physics, Seoul National University, Seoul 08826, Republic of Korea;* orcid.org/0000-0001-5988-5219

Complete contact information is available at: https://pubs.acs.org/10.1021/acs.nanolett.5c01649

Author Contributions

S.M., H.J., K.C., and S.C. conceptualized and designed the experiments. S.M. carried out the device fabrication and characterizations with assistance from H.K. J.Y and J.W.S. analyzed the XPS data. The theoretical calculations were performed by J.-K.K., with the help of K.C. DFT simulations were conducted by D.C. TEM analysis was performed by D.H.K. All authors discussed the results and contributed to the manuscript, which was written by S.M., K.C., and S.C., with input from T.L. and H.J.

Notes

The authors declare no competing financial interest.

■ ACKNOWLEDGMENTS

The authors appreciate the financial support from the National Research Foundation of Korea (NRF) grant funded by the government of the Republic of Korea (the Ministry of Science and ICT) (Nos. NRF-2023R1A2C2003247, 2021R1C1C2091728). This work was also supported by the National Research Foundation of Korea (NRF) grant funded by the Korea government (MSIT) (No. RS-2024-00402972) and the National Research Council of Science & Technology (NST) grant by the Korea government (MSIT) (CRC22031-000).

■ REFERENCES

(1) Dutta, R.; Bala, A.; Sen, A.; Spinazze, M. R.; Park, H.; Choi, W.; Yoon, Y.; Kim, S. Optical Enhancement of Indirect Bandgap 2D Transition Metal Dichalcogenides for Multi-Functional Optoelectronic Sensors. *Adv. Mater.* **2023**, *35* (46), No. 2303272.
(2) Li, J.; Yang, R.; Higashitarumizu, N.; Dai, S.; Wu, J.; Javey, A.; Grigoropoulos, C. P. Transient Nanoscopy of Exciton Dynamics in 2D Transition Metal Dichalcogenides. *Adv. Mater.* **2024**, *36* (21), No. 2311568.
(3) Sangwan, V. K.; Lee, H.-S.; Bergeron, H.; Balla, I.; Beck, M. E.; Chen, K.-S.; Hersam, M. C. Multi-Terminal Memtransistors from Polycrystalline Monolayer Molybdenum Disulfide. *Nature* **2018**, *554* (7693), 500−504.
(4) Jariwala, D.; Marks, T. J.; Hersam, M. C. Mixed-Dimensional van Der Waals Heterostructures. *Nat. Mater.* **2017**, *16* (2), 170−181.
(5) Uddin, S. Z.; Higashitarumizu, N.; Kim, H.; Rahman, I. K. M. R.; Javey, A. Efficiency Roll-Off Free Electroluminescence from Monolayer WSe2. *Nano Lett.* **2022**, *22* (13), 5316−5321.
(6) Park, S.; Schultz, T.; Han, A.; Aljarb, A.; Xu, X.; Beyer, P.; Opitz, A.; Ovsyannikov, R.; Li, L.-J.; Meissner, M.; Yamaguchi, T.; Kera, S.; Amsalem, P.; Koch, N. Electronic Band Dispersion Determination in Azimuthally Disordered Transition-Metal Dichalcogenide Monolayers. *Commun. Phys.* **2019**, *2* (1), 1−6.
(7) Park, S.; Schultz, T.; Xu, X.; Wegner, B.; Aljarb, A.; Han, A.; Li, L.-J.; Tung, V. C.; Amsalem, P.; Koch, N. Demonstration of the Key Substrate-Dependent Charge Transfer Mechanisms between Monolayer MoS_2 and Molecular Dopants. *Commun. Phys.* **2019**, *2* (1), 1−8.
(8) Dresselhaus, M. S.; Chen, G.; Tang, M. Y.; Yang, R. G.; Lee, H.; Wang, D. Z.; Ren, Z. F.; Fleurial, J.-P.; Gogna, P. New Directions for Low-Dimensional Thermoelectric Materials. *Adv. Mater.* **2007**, *19* (8), 1043−1053.
(9) Li, W.; Zhang, X.; Liu, H.; Shu, M.; Zhang, C.; Zong, P. Two-Dimensional van Der Waals Stack Heterostructures for Flexible Thermoelectrics. *Nano Energy* **2024**, *125*, No. 109605.
(10) Kanahashi, K.; Pu, J.; Takenobu, T. 2D Materials for Large-Area Flexible Thermoelectric Devices. *Adv. Energy Mater.* **2020**, *10* (11), No. 1902842.
(11) Hwang, S.; Jang, D.; Lee, B.; Ryu, Y.-S.; Kwak, J.; Kim, H.; Chung, S. All Direct Ink Writing of 3D Compliant Carbon Thermoelectric Generators for High-Energy Conversion Efficiency. *Adv. Energy Mater.* **2023**, *13* (23), No. 2204171.
(12) Park, K. T.; Cho, Y. S.; Jeong, I.; Jang, D.; Cho, H.; Choi, Y.; Lee, T.; Ko, Y.; Choi, J.; Hong, S. Y.; Oh, M.-W.; Chung, S.; Park, C. R.; Kim, H. Highly Integrated, Wearable Carbon-Nanotube-Yarn-Based Thermoelectric Generators Achieved by Selective Inkjet-Printed Chemical Doping. *Adv. Energy Mater.* **2022**, *12* (25), No. 2200256.
(13) Cho, H.; Jang, D.; Yoon, J.; Ryu, Y.-S.; Lee, B.; Lee, B.; Chung, S.; Hong, Y. Milliwatt-Scale Body-Heat Harvesting Using Stretchable Thermoelectric Generators for Fully Untethered, Self-Sustainable Wearables. *ACS Energy Lett.* **2023**, *8* (6), 2585−2594.
(14) Park, S. H.; Jo, S.; Kwon, B.; Kim, F.; Ban, H. W.; Lee, J. E.; Gu, D. H.; Lee, S. H.; Hwang, Y.; Kim, J.-S.; Hyun, D.-B.; Lee, S.; Choi, K. J.; Jo, W.; Son, J. S. High-Performance Shape-Engineerable Thermoelectric Painting. *Nat. Commun.* **2016**, *7* (1), No. 13403.
(15) Kim, F.; Kwon, B.; Eom, Y.; Lee, J. E.; Park, S.; Jo, S.; Park, S. H.; Kim, B.-S.; Im, H. J.; Lee, M. H.; Min, T. S.; Kim, K. T.; Chae, H. G.; King, W. P.; Son, J. S. 3D Printing of Shape-Conformable Thermoelectric Materials Using All-Inorganic Bi2Te3-Based Inks. *Nat. Energy* **2018**, *3* (4), 301−309.
(16) Linseis, V.; Völklein, F.; Reith, H.; Woias, P.; Nielsch, K. Platform for In-Plane ZT Measurement and Hall Coefficient Determination of Thin Films in a Temperature Range from 120 K up to 450 K. *J. Mater. Res.* **2016**, *31* (20), 3196−3204.
(17) Shin, H. S.; Hamdou, B.; Reith, H.; Osterhage, H.; Gooth, J.; Damm, C.; Rellinghaus, B.; Pippel, E.; Nielsch, K. The Surface-to-Volume Ratio: A Key Parameter in the Thermoelectric Transport of Topological Insulator Bi 2 Se 3 Nanowires. *Nanoscale* **2016**, *8* (28), 13552−13557.
(18) Wang, Y.; Yang, L.; Shi, X.-L.; Shi, X.; Chen, L.; Dargusch, M. S.; Zou, J.; Chen, Z.-G. Flexible Thermoelectric Materials and Generators: Challenges and Innovations. *Adv. Mater.* **2019**, *31* (29), No. 1807916.
(19) Cutler, M.; Mott, N. F. Observation of Anderson Localization in an Electron Gas. *Phys. Rev.* **1969**, *181* (3), 1336−1340.
(20) Feng, J.; Li, J.; Liu, R. Low-Temperature Thermoelectric Materials and Applications. *Nano Energy* **2024**, *126*, No. 109651.
(21) Hong, J.; Lee, C.; Park, J.-S.; Shim, J. H. Control of Valley Degeneracy in Mo S 2 by Layer Thickness and Electric Field and Its Effect on Thermoelectric Properties. *Phys. Rev. B* **2016**, *93* (3), No. 035445.
(22) Babaei, H.; Khodadadi, J. M.; Sinha, S. Large Theoretical Thermoelectric Power Factor of Suspended Single-Layer MoS_2. *Appl. Phys. Lett.* **2014**, *105* (19), No. 193901.
(23) Wu, J.; Schmidt, H.; Amara, K. K.; Xu, X.; Eda, G.; Özyilmaz, B. Large Thermoelectricity *via* Variable Range Hopping in Chemical Vapor Deposition Grown Single-Layer MoS_2. *Nano Lett.* **2014**, *14* (5), 2730−2734.
(24) Kang, K.; Xie, S.; Huang, L.; Han, Y.; Huang, P. Y.; Mak, K. F.; Kim, C.-J.; Muller, D.; Park, J. High-Mobility Three-Atom-Thick Semiconducting Films with Wafer-Scale Homogeneity. *Nature* **2015**, *520* (7549), 656−660.

(25) Ohta, H.; Kim, S. W.; Kaneki, S.; Yamamoto, A.; Hashizume, T. High Thermoelectric Power Factor of High-Mobility 2D Electron Gas. *Advanced Science* **2018**, *5* (1), No. 1700696.
(26) Zhang, X.; Pei, Y. Manipulation of Charge Transport in Thermoelectrics. *npj Quant Mater.* **2017**, *2* (1), 68.
(27) Mao, Y.; Fang, Y.; Yuan, K.; Huang, F. Effect of Vanadium Doping on the Thermoelectric Properties of MoS_2. *J. Alloys Compd.* **2022**, *903*, No. 163921.
(28) Guo, H.-H.; Yang, T.; Tao, P.; Zhang, Z.-D. Theoretical Study of Thermoelectric Properties of MoS_2. *Chinese Phys. B* **2014**, *23* (1), No. 017201.
(29) Reed-Lingenfelter, S. N.; Chen, Y.; Yarali, M.; Charboneau, D. J.; Curley, J. B.; Hynek, D. J.; Wang, M.; Williams, N. L.; Hazari, N.; Quek, S. Y.; Cha, J. J. Compact Super Electron-Donor to Monolayer MoS_2. *Nano Lett.* **2022**, *22* (11), 4501−4508.
(30) Kim, J.-K.; Cho, K.; Jang, J.; Baek, K.-Y.; Kim, J.; Seo, J.; Song, M.; Shin, J.; Kim, J.; Parkin, S. S. P.; Lee, J.-H.; Kang, K.; Lee, T. Molecular Dopant-Dependent Charge Transport in Surface-Charge-Transfer-Doped Tungsten Diselenide Field Effect Transistors. *Adv. Mater.* **2021**, *33* (44), No. 2101598.
(31) Kim, S. M.; Jang, J. H.; Kim, K. K.; Park, H. K.; Bae, J. J.; Yu, W. J.; Lee, I. H.; Kim, G.; Loc, D. D.; Kim, U. J.; Lee, E.-H.; Shin, H.-J.; Choi, J.-Y.; Lee, Y. H. Reduction-Controlled Viologen in Bisolvent as an Environmentally Stable n-Type Dopant for Carbon Nanotubes. *J. Am. Chem. Soc.* **2009**, *131* (1), 327−331.
(32) Kiriya, D.; Tosun, M.; Zhao, P.; Kang, J. S.; Javey, A. Air-Stable Surface Charge Transfer Doping of MoS_2 by Benzyl Viologen. *J. Am. Chem. Soc.* **2014**, *136* (22), 7853−7856.
(33) Patil, S. B.; Sankeshwar, N. S.; Mulimani, B. G. Role of Charged Impurities in Thermoelectric Transport in Molybdenum Disulfide Monolayers. *J. Phys.: Condens. Matter* **2017**, *29* (48), No. 485303.
(34) Masselink, W. T. Ionized-Impurity Scattering of Quasi-Two-Dimensional Quantum-Confined Carriers. *Phys. Rev. Lett.* **1991**, *66* (11), 1513−1516.
(35) Neophytou, N.; Thesberg, M. Modulation Doping and Energy Filtering as Effective Ways to Improve the Thermoelectric Power Factor. *J. Comput. Electron* **2016**, *15* (1), 16−26.
(36) Jang, J.; Kim, J.-K.; Shin, J.; Kim, J.; Baek, K.-Y.; Park, J.; Park, S.; Kim, Y. D.; Parkin, S. S. P.; Kang, K.; Cho, K.; Lee, T. Reduced Dopant-Induced Scattering in Remote Charge-Transfer-Doped MoS_2 Field-Effect Transistors. *Sci. Adv.* **2022**, *8* (38), No. eabn3181.
(37) Lee, D.; Lee, J. J.; Kim, Y. S.; Kim, Y. H.; Kim, J. C.; Huh, W.; Lee, J.; Park, S.; Jeong, H. Y.; Kim, Y. D.; Lee, C.-H. Remote Modulation Doping in van Der Waals Heterostructure Transistors. *Nat. Electron* **2021**, *4* (9), 664−670.
(38) Singh, M.; Haverinen, H. M.; Dhagat, P.; Jabbour, G. E. Inkjet Printing—Process and Its Applications. *Adv. Mater.* **2010**, *22* (6), 673−685.
(39) Chung, S.; Cho, K.; Lee, T. Recent Progress in Inkjet-Printed Thin-Film Transistors. *Advanced Science* **2019**, *6* (6), No. 1801445.
(40) Jeong, I.; Cho, K.; Yun, S.; Shin, J.; Kim, J.; Kim, G. T.; Lee, T.; Chung, S. Tailoring the Electrical Characteristics of MoS_2 FETs through Controllable Surface Charge Transfer Doping Using Selective Inkjet Printing. *ACS Nano* **2022**, *16* (4), 6215−6223.
(41) Reed-Lingenfelter, S. N.; Chen, Y.; Yarali, M.; Charboneau, D. J.; Curley, J. B.; Hynek, D. J.; Wang, M.; Williams, N. L.; Hazari, N.; Quek, S. Y.; Cha, J. J. Compact Super Electron-Donor to Monolayer MoS_2. *Nano Lett.* **2022**, *22* (11), 4501−4508.
(42) Matsuyama, K.; Aoki, R.; Miura, K.; Fukui, A.; Togawa, Y.; Yoshimura, T.; Fujimura, N.; Kiriya, D. Metallic Transport in Monolayer and Multilayer Molybdenum Disulfides by Molecular Surface Charge Transfer Doping. *ACS Appl. Mater. Interfaces.* **2022**, *14* (6), 8163−8170.
(43) Zhang, X.; Shao, Z.; Zhang, X.; He, Y.; Jie, J. Surface Charge Transfer Doping of Low-Dimensional Nanostructures toward High-Performance Nanodevices. *Adv. Mater.* **2016**, *28* (47), 10409−10442.
(44) Chamlagain, B.; Withanage, S. S.; Johnston, A. C.; Khondaker, S. I. Scalable Lateral Heterojunction by Chemical Doping of 2D TMD Thin Films. *Sci. Rep* **2020**, *10* (1), No. 12970.
(45) Radisavljevic, B.; Kis, A. Mobility Engineering and a Metal−Insulator Transition in Monolayer MoS_2. *Nat. Mater.* **2013**, *12* (9), 815−820.
(46) Wang, D.; Li, X.-B.; Sun, H.-B. Modulation Doping: A Strategy for 2D Materials Electronics. *Nano Lett.* **2021**, *21* (14), 6298−6303.
(47) Sun, P.; Wei, B.; Zhang, J.; Tomczak, J. M.; Strydom, A. M.; Søndergaard, M.; Iversen, B. B.; Steglich, F. Large Seebeck Effect by Charge-Mobility Engineering. *Nat. Commun.* **2015**, *6* (1), 7475.
(48) Chaves, F. A.; Feijoo, P. C.; Jimenez, D. 2D pn Junctions Driven Out-of-Equilibrium. *Nanoscale Advances* **2020**, *2* (8), 3252−3262.
(49) Jeong, I.; Yang, J.; Jang, J.; Cho, D.; Kwon, D.-H.; Kim, J.-K.; Lee, T.; Cho, K.; Chung, S. Charged-Impurity Free Printing-Based Diffusion Doping in Molybdenum Disulfide Field-Effect Transistors. *arXiv Preprint*, arXiv:2407.21678, 2024. DOI: 10.48550/arXiv.2407.21678
(50) Greczynski, G.; Hultman, L. X-Ray Photoelectron Spectroscopy: Towards Reliable Binding Energy Referencing. *Prog. Mater. Sci.* **2020**, *107*, No. 100591.
(51) Mitta, S. B.; Choi, M. S.; Nipane, A.; Ali, F.; Kim, C.; Teherani, J. T.; Hone, J.; Yoo, W. J. Electrical Characterization of 2D Materials-Based Field-Effect Transistors. *2D Mater.* **2021**, *8* (1), No. 012002.
(52) Ng, H. K.; Chi, D.; Hippalgaonkar, K. Effect of Dimensionality on Thermoelectric Powerfactor of Molybdenum Disulfide. *J. Appl. Phys.* **2017**, *121* (20), No. 204303.
(53) Hippalgaonkar, K.; Wang, Y.; Ye, Y.; Qiu, D. Y.; Zhu, H.; Wang, Y.; Moore, J.; Louie, S. G.; Zhang, X. High thermoelectric power factor in two-dimensional crystals of MoS_2. *Phys. Rev. B* **2017**, *95* (11), No. 115407.
(54) Xu, K.; Ruoko, T.; Shokrani, M.; Scheunemann, D.; Abdalla, H.; Sun, H.; Yang, C.; Puttisong, Y.; Kolhe, N. B.; Figueroa, J. S. M.; Pedersen, J. O.; Ederth, T.; Chen, W. M.; Berggren, M.; Jenekhe, S. A.; Fazzi, D.; Kemerink, M.; Fabiano, S. On the Origin of Seebeck Coefficient Inversion in Highly Doped Conducting Polymers. *Adv. Funct Materials* **2022**, *32* (20), No. 2112276.
(55) Pichanusakorn, P.; Bandaru, P. Nanostructured Thermoelectrics. *Materials Science and Engineering: R: Reports* **2010**, *67* (2−4), 19−63.
(56) Xie, H.; Su, X.; Bailey, T. P.; Zhang, C.; Liu, W.; Uher, C.; Tang, X.; Kanatzidis, M. G. Anomalously Large Seebeck Coefficient of $CuFeS_2$ Derives from Large Asymmetry in the Energy Dependence of Carrier Relaxation Time. *Chem. Mater.* **2020**, *32* (6), 2639−2646.
(57) Hwang, E. H.; Das Sarma, S. Screening-Induced Temperature-Dependent Transport in Two-Dimensional Graphene. *Phys. Rev. B* **2009**, *79* (16), No. 165404.
(58) Ma, N.; Jena, D. Charge Scattering and Mobility in Atomically Thin Semiconductors. *Phys. Rev. X* **2014**, *4* (1), No. 011043.
(59) Li, Q.; Hwang, E. H.; Das Sarma, S. Disorder-Induced Temperature-Dependent Transport in Graphene: Puddles, Impurities, Activation, and Diffusion. *Phys. Rev. B* **2011**, *84* (11), No. 115442.
(60) Pu, J.; Kanahashi, K.; Cuong, N. T.; Chen, C.-H.; Li, L.-J.; Okada, S.; Ohta, H.; Takenobu, T. Enhanced Thermoelectric Power in Two-Dimensional Transition Metal Dichalcogenide Monolayers. *Phys. Rev. B* **2016**, *94* (1), No. 014312.
(61) Park, N.-W.; Lee, H.; Choi, J.-W.; Shin, H.; Kang, M.-S.; Kim, S.-H.; Cho, J.-M.; Kim, M.-J.; Kim, G.-S.; Lee, S.-K. Temperature-Dependent Thermal Transport of Polycrystalline van Der Waals Semimetallic $PtSe_2$ Films. *J. Phys. Chem. C* **2023**, *127* (28), 13556−13561.
(62) Kim, S.-H.; Kang, M.-S.; Choi, J.-W.; Cho, J.-M.; Kim, Y.-H.; Park, N.-W.; Kim, G.-S.; Lee, S.-K. Thickness-Dependent In-Plane Thermoelectric Properties of $PtTe_2$ with n-Type Conduction. *J. Phys. Chem. C* **2023**, *127* (3), 1673−1679.
(63) Choi, J. W.; Lee, W.-Y.; Kim, S.-H.; Kang, M.-S.; Cho, J.-M.; Park, N.-W.; Kwon, H. J.; Kim, Y.-H.; Kim, G.-S.; Yoon, Y.-G.; Lee, S.-K. Interface-Driven Seebeck Effect in Two-Dimensional Trilayer-Stacked $PtTe_2/MoS_2/MoS_2$ Heterostructures *via* Electron−Electron Interactions. *Nano Energy* **2023**, *115*, No. 108713.

(64) Xin, N.; Tang, G.; Lan, T.; Li, Y.; Kou, J.; Zhang, M.; Zhao, X.; Nie, Y. Improving the Thermoelectric Performance of Cu-Doped MoS_2 Film by Band Structure Modification and Microstructural Regulation. *Appl. Surf. Sci.* **2023**, *611*, No. 155611.
(65) Lee, W.; Kang, M.; Choi, J. W.; Kim, S.; Park, N.; Kim, G.; Kim, Y.; Lee, S. Alternatingly Stacked Low- and High-Resistance $PtSe_2$ /$PtSe_2$ Homostructures Boost Thermoelectric Power Factors. *Adv. Elect Materials* **2023**, *9* (8), No. 2300170.
(66) Kang, M.-S.; Kang, S.-Y.; Lee, W.-Y.; Park, N.-W.; Kown, K. C.; Choi, S.; Kim, G.-S.; Nam, J.; Kim, K. S.; Saitoh, E.; Jang, H. W.; Lee, S.-K. Large-Scale MoS_2 Thin Films with a Chemically Formed Holey Structure for Enhanced Seebeck Thermopower and Their Anisotropic Properties. *J. Mater. Chem. A* **2020**, *8* (17), 8669−8677.

https://doi.org/10.1021/acs.nanolett.5c01649
Nano Lett. 2025, 25, 9994−10002